Chemical Engineering Journal 428 (2022) 131793

Contents lists available at ScienceDirect

Chemical Engineering Journal

journal homepage: www.elsevier.com/locate/cej

Liquid or solid? a biologically inspired concentrated suspension for protective coating

Yuxuan Wu [a], Wenhui Wang [a], Junshuo Zhang [a], Min Sang [a], Yunqi Xu [a], Jianyu Zhou [a], Sheng Wang [a,*], Yibing Cai [b], Shouhu Xuan [a], Xinglong Gong [a,*]

[a] CAS Key Laboratory of Mechanical Behavior and Design of Materials, Department of Modern Mechanics, CAS Center for Excellence in Complex System Mechanics, University of Science and Technology of China, Hefei, Anhui 230027, China
[b] Key Laboratory of Eco-textiles, Ministry of Education, Jiangnan University, Wuxi China 214122, PR China

ARTICLE INFO

Keywords:
Concentrated suspension
Shear thickening
High-temperature tolerant
Liquid-to-solid
Anti-impact

ABSTRACT

Thermophiles can survive in a high-temperature environment due to the synergy of hydrophobic interaction and electrostatic interaction in their proteins. Shear thickening fluid (STF) is a kind of concentrated suspension, which shows shear thickening (ST) behavior and can transform from a liquid state to a solid state under shearing. However, this special phenomenon relies on the hydrogen bonds between particles and dispersing medium. At elevated temperatures, the hydrogen bonds will break and the ST effect will become weaker or even disappear. Herein, inspired by the high-temperature resistance mechanism of thermophile proteins, a novel MOF-801 based STF with better ST effect at elevated temperatures is reported. Specifically, the hydrogen bonds that conventional STF relies on are replaced with hydrophobic interaction and electrostatic interaction, adopting a strategy of dispersing MOF-801 into a mixture containing poly(ethylene glycol), poly(acrylic acid), and Ca^{2+}. When the temperature rises to 55 ℃, the storage modulus of M-STF rises from 13 Pa to 2036 Pa, and the suspension transforms to a solid-like state. Thus, a shapeable, self-healing, shear-stiffing, and conductive polymer-like substance can be obtained. In addition, a high-performance composite can be developed by impregnating M-STF into Kevlar, which shows promising applications in lightweight body protection.

1. Introduction

In nature, as the temperature rises, substances generally change from solid to liquid or from liquid to gas, such as the melting of ice and the evaporation of water. In other words, the internal structure of the substance tends to be disordered at elevated temperatures. However, some materials are thermally stable and can maintain their structures even at elevated temperatures. For instance, thermophile bacteria can live in extremely elevated temperature environments (between 40 ~ 120 ℃) like deep-sea hydrothermal vents because of their special thermally stable proteins. Unlike proteins of other normal animals, proteins of thermophiles possess more charged amino acid residues, which can provide electrostatic and hydrophobic interaction (Fig. 1a, b). When the temperature rises, the hydrophobic residues will dehydrate, which reduces the permittivity nearby [1,2] and enhances electrostatic interactions between charged residues, as a result, the protein can keep its structure stable at an elevated temperature [3,4].

Shear thickening fluid (STF) is a kind of concentrated suspension that consists of dispersing phase particles and dispersing medium [5–7]. Once the applied shear rate reaches its critical value, STF's viscosity will increase rapidly as the shear rate increases. Because of its special shear thickening (ST) behavior, STF has been used in various fields, such as damper, liquid body armor, sports shoe cushioning, etc. [8,9]. Particularly, STF treated fabrics are widely studied in recent years for their potential application in body protection [10–12]. Liu et al. [10] demonstrated that Kevlar intercalated with STF can greatly enhance the fabric's cut and puncture resistance. So far, various mechanisms, such as order-disorder transition, hydrocluster, and contact rheology model, have been developed to explain the ST behavior [13–15]. Specifically, many STFs exhibit a discontinuous shear thickening (DST), in which the stress suddenly jumps with increasing shear rate, marking a transition from a flow state where particles remain well separated by lubrication layers to one dominated by frictional contacts [16–18]. The contact rheology model believes that when DST occurs, the liquid film between particles cannot maintain separation. Thus, the interaction force between particles undergoes a lubricated-to-frictional transition and they

* Corresponding authors.
E-mail addresses: wsh160@ustc.edu.cn (S. Wang), gongxl@ustc.edu.cn (X. Gong).

https://doi.org/10.1016/j.cej.2021.131793
Received 1 June 2021; Received in revised form 26 July 2021; Accepted 8 August 2021
Available online 14 August 2021

can agglomerate to form a frictional contact network under loading [19–23]. The network can withstand the applied shear force, leading to an increase in viscosity and yield stress. In other words, it is the formation of frictional contact networks that leads to the transition of STF from liquid state to jammed solid state [20,21,24].

However, conventional STFs are prepared by dispersing SiO_2 in poly (ethylene glycol) or ethylene glycol, and the occurrence of shear thickening mainly relies on the hydrogen bonds between the particles and the medium and the formation of frictional contact networks [25,26]. When the temperature rises, hydrogen bonds tend to be broken and frictional contact networks cannot be formed, leading to a weaker or even disappearance of ST effect (Fig. 1c) [27], which greatly limits its application. Therefore, to achieve the above-mentioned liquid-to-solid transition as temperature rises and overcome the drawback of STF's elevated-temperature intolerance, the internal particle forces must be replaced. If STF can form micro-structures similar to the frictional contact network during the heating process, its liquid-to-solid transformation may be occurred.

Inspired by the molecular mechanism of thermally stable thermophile proteins, a concentrated suspension that could transform from liquid to solid at elevated temperatures was prepared. MOF-801, which was rich in carboxyl groups on the surface, was used as the dispersing phase and added to the poly(ethylene glycol)200 (PEG200). By introducing poly(acrylic acid) (PAA) and Ca^{2+} into the dispersing medium, the hydrogen bond, which was the internal force that traditional STF relied on, was replaced with hydrophobic interaction and ionic interaction. For the first time, a novel MOF-801 based STF (M-STF) with enhanced ST behavior in elevated temperature was developed. At 55 ℃, the interaction between particles was improved, forming cages that could trap PEG200 in, and these cages connected to each other to build-up a structure which was similar to the frictional contact network in DST (M-frictional contact network). As a result, the suspension transformed from liquid to solid state.

2. Material and methods

All chemical reagents were purchased from commercial sources and used without further purification: fumaric acid (AR), $Ca(NO_3)_2{\cdot}4H_2O$ (AR), formic acid (98%), poly(ethylene glycol) 200 (PEG200, AR), and ethanol (AR) were supplied by Sinopharm Chemical Reagent Co., Ltd. Zirconium chloride ($ZrCl_4$, 98%) and Poly(acrylic acid) (PAA, $M_w \sim 2000$) was purchased from Aladdin. The plain weave Kevlar 129 (200 g/m^2) was got from Beijing Junantai Protection Technology Co., Ltd.

2.1. Experimental

Synthesis of MOF-801 particles: Firstly, 21.5 g of $ZrCl_4$ was dissolved in water (300 mL) under stirring. Then, formic acid (120 mL), fumaric acid (10.5 g) and another 150 mL of water were added into the solution. The reaction was kept for 24 h, and then the particles were collected and washed. The obtained MOF-801 was put in vacuum for 12 h.

Preparation of the M-STF: Firstly, a certain amount of PAA was dissolved in PEG200 to obtain a clear solution. Then, MOF-801 was added into the solution and dispersed by ball milling to obtain a concentrated suspension. The introduction of Ca^{2+} was achieved by adding $Ca(NO_3)_2{\cdot}4H_2O$ into the above-mentioned concentrated suspension. After ball milling, M-STF was obtained.

Preparation of M-STF/Kevlar: M-STF/Kevlar composite was prepared by a simple "dilution-soaking-drying" method. Briefly, M-STF was diluted with ethanol at a volume ratio of 1:5 and ultrasonicated for 40 min to obtain a homogeneous solution. Subsequently, Kevlar was impregnated in the diluted solution for 2 min, and the soaked fabric was placed at a fume hood to evaporate the ethanol. By repeating "soaking-drying" process, M-STF/Kevlar composites with different mass fractions were obtained.

2.2. Characterization

The rheological properties of M-STF were characterized on an Anton Paar's Physical MCR302 at different temperatures. At the dynamic shear tests, a plate-to-plate rotor (PP20) was used, the gap size and shear strain were kept as 1 mm and 0.1%, respectively.

The microstructures of MOF-801 were visualized by SEM (Sirion200) and TEM (HT7700, Japan). X-ray diffraction (XRD) patterns and infrared (IR) spectra of MOF-801 were obtained on an X-ray diffractometer (XRD, Smartlab, Rigaku, Japan) and a Nicolet Model 759 Fourier transform infrared (FT-IR) spectrometer, respectively. Thermal stabilities of MOF-801 and the suspensions were investigated by a DTG-60H and the heating rate was 10 °C/min and 2 °C/min, respectively. To

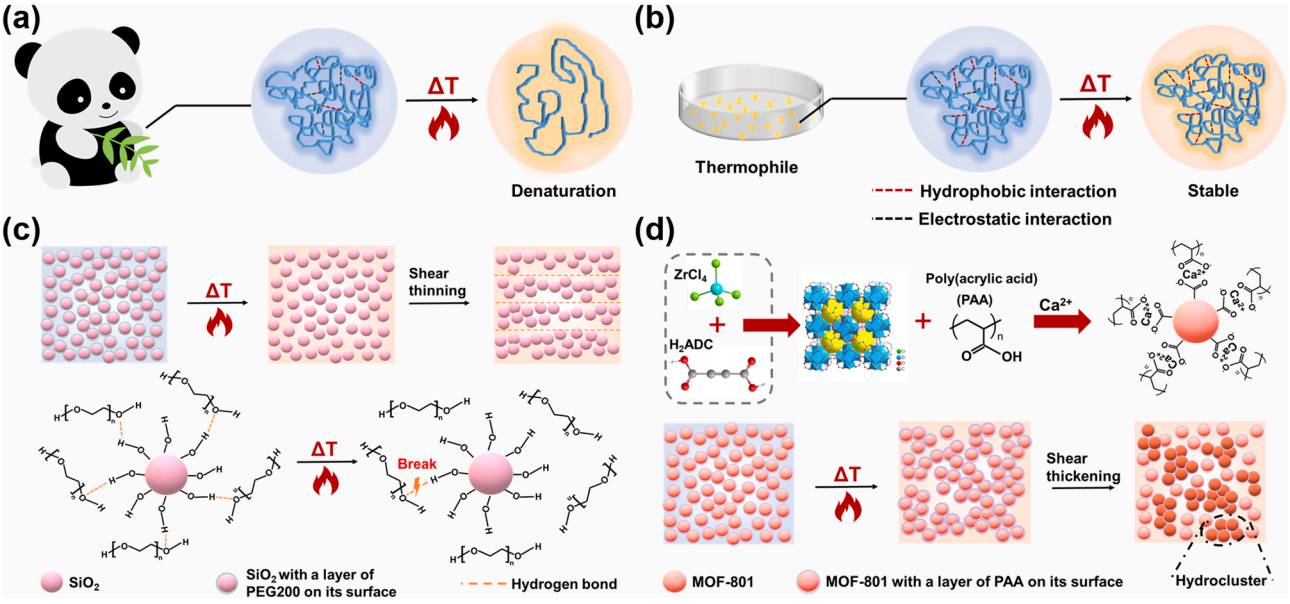

Fig. 1. (a) Proteins of normal animals will denature at elevated temperature; (b) The thermophile protein is thermally stable; As the temperature rises, (c) the ST effect of conventional STF disappears while (d) M-STF shows better ST behavior.

evaluate the Brunauer-Emmett-Teller (BET) surface area of MOF-801, the particles were activated at 100 °C for 5 h under vacuum and then the test was carried on a Micromeritics Tristar II 3020 M.

Yarn pull-out test: To study the interaction between yarns in fabric, yarn pull-out tests were carried out on a universal tensile instrument (MTS, Criterion^{TM} Model 43). During the test, the target yarn (at the center of the fabrics) was clamped by the upper grip of MTS while the other end of this yarn was cut off (Fig. S1a). The pul-out speed varied from 10 ~ 200 mm/min.

Drop hammer test: The failure process of the fabric under low-speed impact was studied on a drop hammer tester (Fig. S1b). The impactor was a steel rounded tip rod (Ø = 10 mm, L = 105 mm) and the total impact load was 2.95 kg. During the experiment, the impactor dropped from different heights, and the acceleration-time diagrams were recorded.

Quasi-static puncture test: MTS was employed to investigate the contact force of M-STF/Kevlar and neat Kevlar fabrics under vertical load. During the test, the fabric was fixed by a clamp with twelve screws and groove structure (Fig. S1c). The rounded tip penetrator (Ø = 8 mm, L = 60 mm) slowly moved downwards at a speed of 2 mm/min to penetrate the center of the sample, and the force–displacement curve was recorded.

Ballistic impact test: The failure process of the fabric under high-speed impact was studied by ballistic impact test. During the test, a spherical steel bullet (Ø = 8 mm, m = 2.08 g) was driven by a gas gun to impact the fabric. The size of the impact area was 85 × 85 mm. The incident speed of the bullet could be adjusted by the air pressure and measured by a photo-electric gate mounted on the muzzle. A high-speed camera was used to record the impact process and assist in calculating the residual velocity of the bullet (Fig. S2).

3. Results and discussion

The SEM and TEM images (Fig. 2a and b) showed that MOF-801 was quasi-spherical with a particle size range of 100 ~ 150 nm. The crystal structure could be characterized by XRD (Fig. 2c), the sharp peaks of as-synthesized MOF-801 matched with the simulation pattern, indicating a high phase purity of the nanocrystals [28]. After being dispersed into PEG200-PAA-Ca^{2+} by ball milling and recollected from the suspension by washing with ethanol, the characteristic peaks of MOF-801 were still the same as simulation result. Thus, the MOF-801 exhibited excellent mechanical stability and its crystal structure remained intact after mixing with PEG200-PAA-Ca^{2+}. MOF-801 possessed a microporous structure and showed type-I isotherms (Fig. 2d), the calculated BET surface area was 746 m^2g^{-1}. The thermal stability of MOF-801 was investigated by TGA (Fig. 2e), and its weight loss could be divided into three stages. The first stage occurred before 100 °C and the weight loss at this stage was attributed to the evaporation of water adsorbed on the surface of particles. The second weight loss could be ascribed to the escape of guest molecules (such as water and ethanol) in the pores of MOF-801. The last stage occurred at 420 °C, which was due to the decomposition of MOF-801, indicating good thermal stability of the particles. The FT-IR spectrum of MOF-801 was shown in Fig. 2f. The peaks at 1557 cm^{-1} and 1385 cm^{-1} indicated the presence of − C = O − O bonds, and the peaks at 1210 cm^{-1} and 1084 cm^{-1} were assigned to the − C − O and − C = O − OH bonds [29], indicating there were − C = O − OH that could coordinate with Ca^{2+} on the surface of MOF-801.

The rheological behavior of dispersing medium (PEG200-PAA-Ca^{2+}) was shown in Fig. 3a, the influence of temperature on the viscosity of PEG200-PAA-Ca^{2+} could be ignored. In the initial shearing stage, the polymer chains stretched under external force, leading to a slight decrease in viscosity. Subsequently, the viscosity did not change significantly as the shear rate increases. When MOF-801 was dispersed into PEG200 directly (MOF-801/PEG200), the particles tended to aggregate together and could not be uniformly dispersed in the medium due to the weak interaction between MOF-801 and PEG200. Therefore, the system appeared as a colloidal gel with poor fluidity, and its viscosity decreased with increasing shear rate and temperature (Fig. 3b). When Ca^{2+} was introduced into the MOF-801/PEG200, the coordination effect led to a more severe aggregation between MOF-801 particles, and the viscosity of the mixture increased dramatically to a gelation state which could not be tested by steady shear (Fig. 3c). Adding a small amount of PAA into PEG200 (1 g PAA was dissolved in 10 mL PEG200) could improve the interaction between particles and dispersing medium: the order of magnitude of initial viscosity dropped from 10^5 to 10^2, and the suspension showed a slight ST effect. However, the ST behavior still

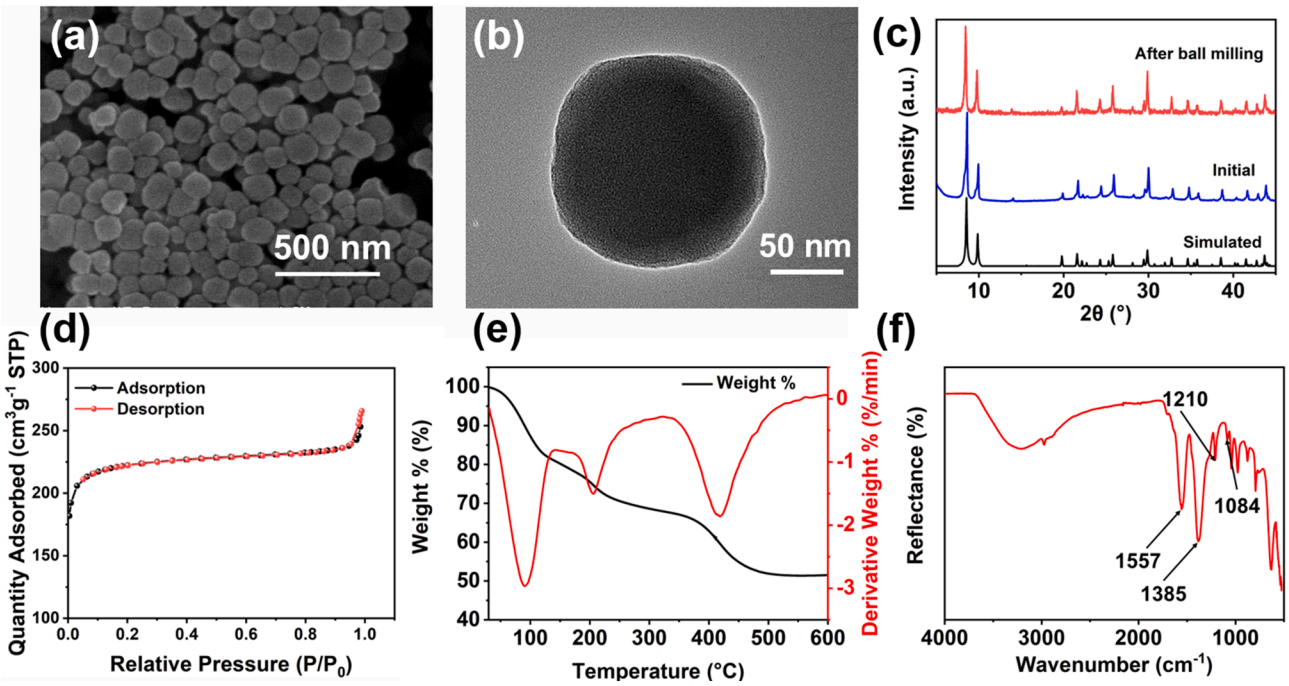

Fig. 2. (a) SEM image, (b) TEM image, (c) XRD patterns, (d) N_2 adsorption-desorption isotherms, (e) TGA curves, and (f) FT-IR spectra of MOF-801 nanoparticles.

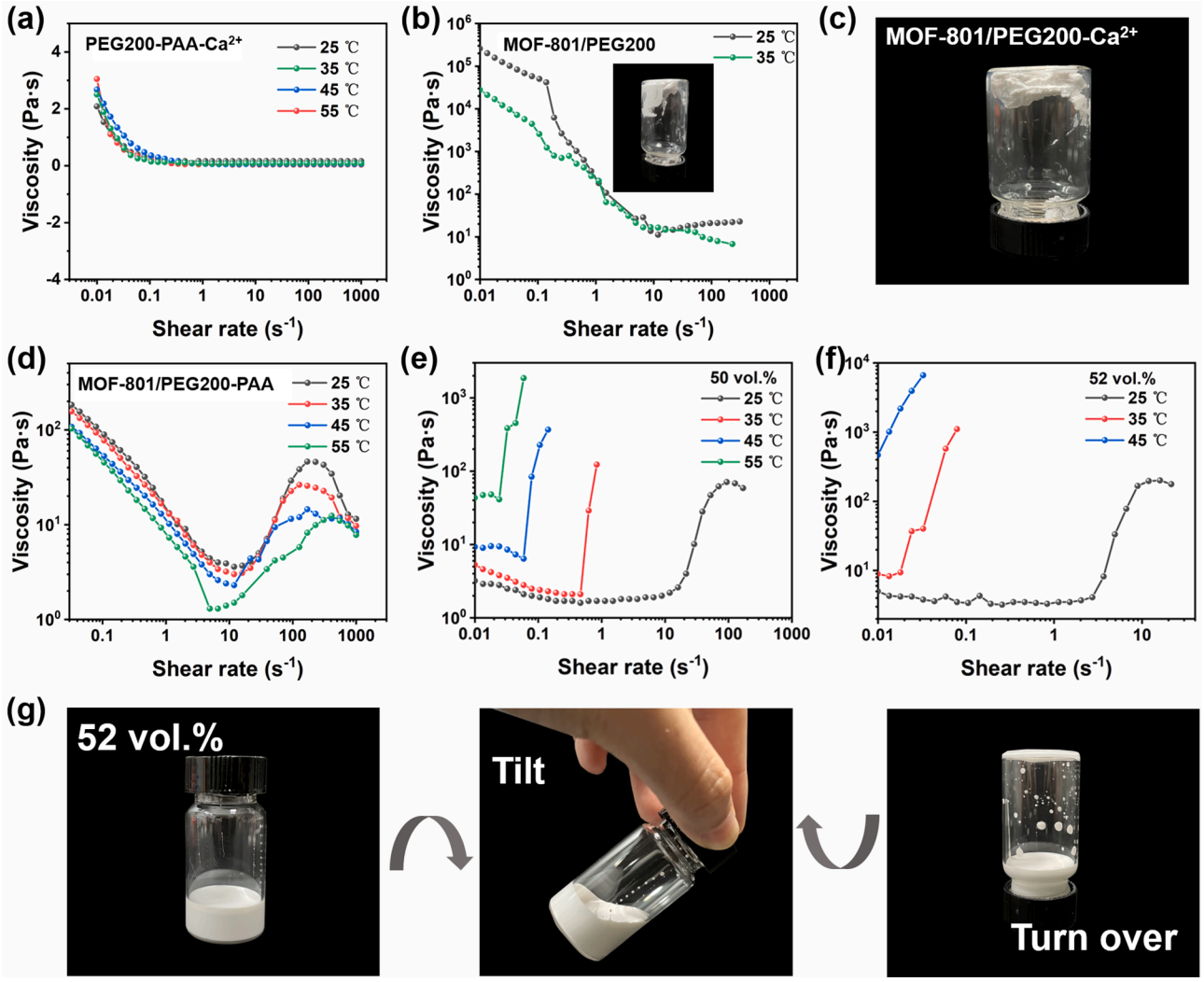

Fig. 3. The curves of viscosity versus shear rate for (a) PEG200-PAA-Ca^{2+}, (b) 50 vol% MOF-801/PEG200, (d) 50 vol% MOF-801/PEG200-PAA, (e) 50 vol% M-STF and (f) 52 vol% M-STF at different temperatures. Photograph of (c) 50 vol% MOF-801/PEG200- $Ca^{2+}$and (g) 52 vol% M-STF.

relied on the hydrogen bonds between particles and dispersing medium. As a result, the ST effect became weaker as temperature increases (Fig. 3d). The interaction between MOF-801 and dispersing medium could be significantly modified when both Ca^{2+} and PAA were added. As shown in Fig. 3e and f, the initial viscosity of the suspension dropped rapidly below 10 Pa·s, showing good fluidity and dramatic ST effect. More importantly, the ST effect became stronger at elevated temperatures. At 25 ℃, the critical shear rate of 50 vol% M-STF was 8.89 s^{-1} and the maximum viscosity was 71 Pa·s. When the temperature rose to 55 ℃, the critical shear rate decreased to 0.024 s^{-1} and the maximum viscosity increased to 1850 Pa·s. It should be pointed out that the low temperature had little effect on hydrophobic interaction and electrostatic interaction, but it could increase the number and the strengths of hydrogen bonds in the suspension [30,31]. Thus, M-STF also exhibited better ST effect at low temperatures (Fig. S3).

The influence of PAA content and [Ca^{2+}] on rheological properties of the suspension was studied. When the content of PAA was too low (Fig. S4a) or too high (Fig. S4b), the ST effect could not increase with increasing temperature. This might be because the low content of PAA could not provide enough coordination sites and the high content of PAA would consume a lot of Ca^{2+}, both of these two conditions could lead to a weak connection between MOF-801 and PAA. As temperature rises, the increased force originated from hydrophobic interaction and electrostatic interaction could not offset the decrease in the force caused by the rupture of hydrogen bonds. Thus, the suspension showed weaker ST behavior at elevated temperatures. As shown in Fig. S4c-f, the optimal concentration of Ca^{2+} was investigated. When the amount of Ca^{2+} was not enough, ST behavior was poorer due to insufficient coordination bonds and weak interaction between particles and media. When [Ca^{2+}] was too high, the coordination sites between the PAA chains increased, which reduced the coordination sites between MOF-801 and PAA, and the interaction between the particles and the medium was relatively decreased, resulting in a poorer ST effect. Thus, the optimal mass ratio of MOF-801, PAA, and $Ca(NO_3)_2{\cdot}4H_2O$ in the suspension was MOF-801: PAA: $Ca(NO_3)_2{\cdot}4H_2O$ = 125: 8.17: 1.

54 vol% M-STF was prepared according to the optimal ratio. As shown in Fig. 4a, its initial and maximum viscosity increased dramatically as the temperature rose. At the same time, the critical shear rate decreased, indicating the suspension was more likely to exhibit stronger ST behavior at an elevated temperature. For instance, when the temperature rose from 25 ℃ to 45 ℃, the maximum viscosity of 54 vol% M-STF could increase from 877 Pa·s to 27577 Pa·s. With further heating, M-STF transformed into a solid-like material (MOF-801 based shear thickening gel, M-STG, Fig. 4b) at 55 ℃. The rate-dependent rheological properties of M-STF and M-STG from 25 ℃ to 75 ℃ were studied (Fig. S5). It was clear that as the shear frequency increased both the storage modulus of M-STF and M-STG showed a gradual upward trend due to the ST effect of the suspension. The initial storage modulus and

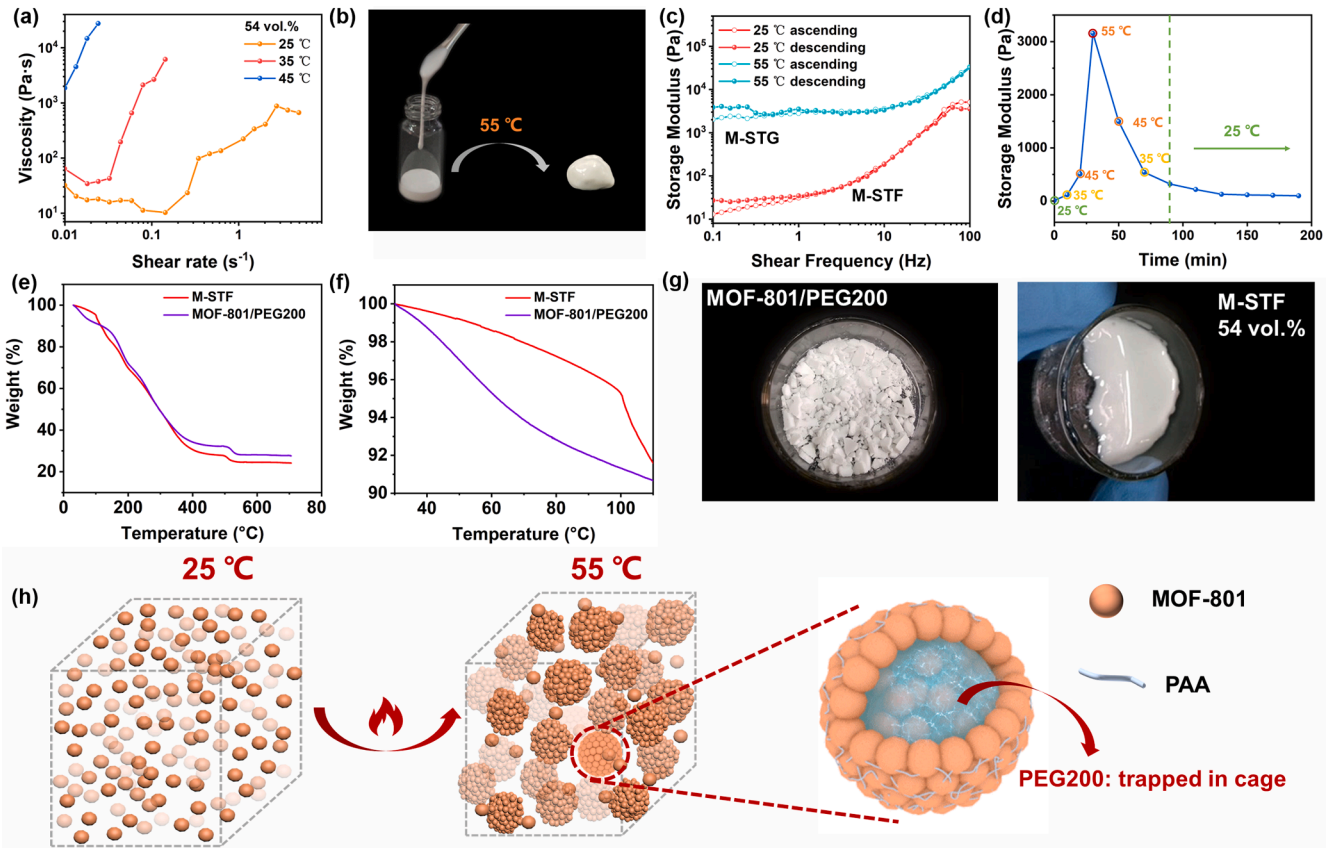

Fig. 4. (a) The curves of viscosity versus shear rate for 54 vol% M-STF. (b) M-STF transformed into M-STG at 55 ℃. (c) Rate-dependent rheological properties of 54 vol% M-STF and M-STG in the shear frequency of 0.1–100 Hz. (d) Reversibility of the thermal hardening concentrated suspension. (e, f) TGA results of M-STF and MOF-801/PEG200. (g) Photograph of MOF-801/PEG200 and M-STF after drying at 80 ℃ for 1.5 h. (h) The illustration of M-STF transforming to M-STG at 55 ℃.

the maximum storage modulus also increased with increasing temperature. However, the storage modulus of M-STG at 75 ℃ was slight lower than the counterpart at 65 ℃. This might be because higher temperature caused the excessive volatilization of PEG200, which destroyed the continuity of the M-STG structure and reduced the storage modulus. Since PEG200 was relatively easier to volatilize at 65 °C and 75 °C, 55 °C was used as the highest temperature in follow studies. When the temperature rose from 25 ℃ to 55 ℃, the initial storage modulus of the suspension increased from 13 Pa to 2036 Pa, and the maximum storage modulus increased from 5077 Pa to 33400 Pa. The reversibility of M-STF and M-STG under cyclic loading were also investigated (Fig. 4c). In the high-frequency region, the storage modulus during the ascending and descending process could be well overlapped, while the storage modulus during the descending process in the low-frequency region will be higher than that in the ascending process. This was because the state of the suspension was dominated by ST effect at high-frequency region where the particles were tightly gathered together to form a robust structure under shearing, and the structural strength was mainly controlled by the magnitude of shearing force. In the low frequency region, the system was close to the equilibrium state, and the particles tended to disperse freely. As a porous particle, the friction between MOF-801 was high. Thus, instead of returning to their initial dispersing state, some particles tended to aggregate together after a cyclic loading, leading to a higher storage modulus compared to the initial counterpart. For example, the initial storage modulus of M-STG was 2036 Pa, and the final storage modulus increased to 3857 Pa after a cyclic loading. The transition from M-STF to M-STG was partially reversible. As shown in Fig. 4d, the storage modulus of the suspension gradually increased from 11 Pa to 3100 Pa as temperature varied from 25 ℃ to 55 ℃. However, the suspension could not return to its initial state in the subsequent cooling process and the storage modulus remained around 100 Pa when the temperature returned to 25 °C, which was resulted from the aggregated particles.

TGA was employed to analyze the weight loss process of 54 vol% M-STF and MOF-801/PEG200 (Fig. 4e and f). As shown in Fig. 4e, the difference in weight loss between M-STF and MOF-801/PEG200 mainly occurred before 100 ℃, where PAA was thermally stable (Fig. S6) and the weight loss could be ascribed to the volatilization of PEG200. In this stage, the volatilization rate of PEG200 in MOF-801/PEG200 was significantly higher than that in M-STF (Fig. 4f). This was because the MOF-801 particles in M-STF aggregated to form some cages under the synergistic effect of hydrophobic interaction and electrostatic force, which trapped the dispersing medium and prevented the evaporation of PEG200 (Fig. 4h). These cages further accumulated to form a structure which was similar to the frictional contact network in DST. As a result, M-STF turned into M-STG. With further heating, PAA decomposed, causing the collapse of cages, thus, M-STF and MOF-801/PEG200 showed similar weight loss behavior. Additionally, the microscopic images of 54 vol% M-STF at room temperature and after 55 ℃ treated were shown in Fig. S7. Clearly, M-STF was a homogeneous liquid at room temperature, while many aggregates could be observed after being treated at 55 ℃. These aggregates were the aforementioned cages. Fig. 4g was the photographs of MOF-801/PEG200 and M-STF after drying at 80 ℃ for 1.5 h. Obviously, MOF-801/PEG200 tended to dry out after the long-term heating, while M-STF could retain most of the liquid composition.

Fig. 5 presented some photographs of M-STG. As shown in Fig. 5a, M-STG behaved like a polymer which was shapeable and self-healing. These two properties originated from the deformable liquid component and the slidable particle skeleton of M-STG. Besides, M-STG was conductive due to the presence of Ca^{2+} and NO_3^- in the dispersing medium. As a concentrated suspension, M-STG crept slowly and could

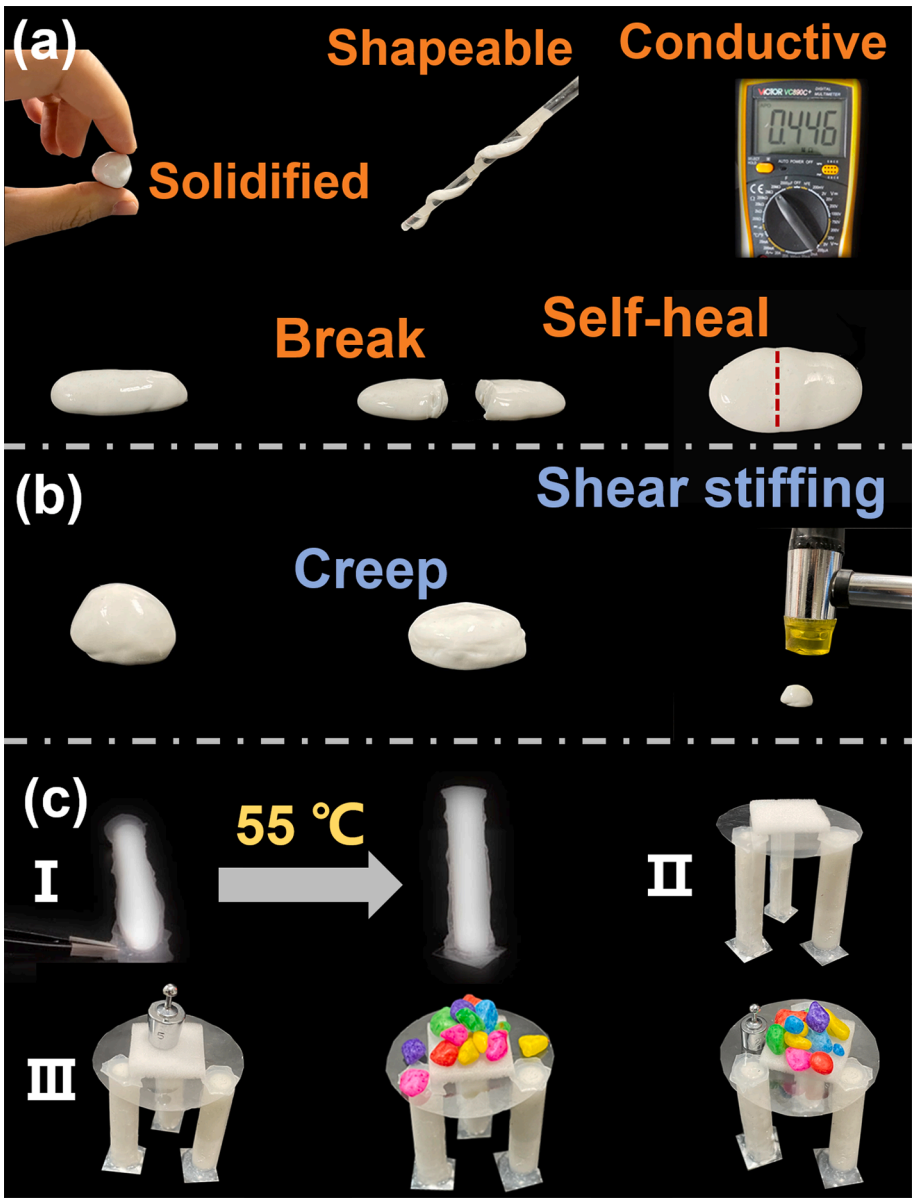

Fig. 5. Photographs of M-STG: (a) M-STG was shapeable, conductive, and self-healing. (b) M-STG crept under static state, and show shear stiffening behavior when it was impacted; (c-I) 54 vol% M-STF was packaged in an eco-flex cylindrical shell and the composite was too soft to keep upright at 25 ℃, however, M-STF transformed into M-STG at 55 ℃, and (c-II) the composite was strong enough to stand up and (c-III) could serve as a table's leg to support objects.

not maintain a fixed three-dimensional shape for a long time. However, when it was impacted, and its structural strength rose sharply to remain a stable shape, in other words, shear stiffening occurred (Fig. 5b). The unique thermal hardening property endowed it with the potential application as a special structural material in elevated-temperature conditions. For example, M-STF was packaged in an eco-flex cylindrical shell (inside diameter of 6 mm, outer diameter of 8 mm and height of 41 mm, Fig. S8) and the composite was soft, flexible and could not keep upright at 25 ℃ (Fig. 5c-I). However, M-STF transformed into M-STG at 55 ℃, and the composite was strong enough to stand up (Fig. 5c-II) and could serve as table legs to support objects (Fig. 5c-III).

The 54 vol% M-STF was used to impregnate Kevlar and prepare M-STF/Kevlar composite by a simple "dilution-soaking-drying" method. Fig. 6 exhibited the SEM images of neat Kevlar (a) and M-STF/Kevlar composite (b–d). Compared to the neat fabric, the surfaces of the M-STF/Kevlar were rougher and M-STF was evenly wrapped on the surface of yarns, indicating a good impregnation result.

To investigate the best impregnation mass fraction of M-STF and friction between fabric yarns, yarn pull-out tests were carried out at room temperature [32]. As shown in Fig. 7a, the maximum pull-out force (F_{max}) of the neat Kevlar was about 2.2 N, which was independent of the pull speed. Additionally, the pull-out force of the Kevlar treated by PEG200-PAA-Ca^{2+} showed similar properties to neat Kevlar (Fig. S9). The F_{max} of it was about 2.6 N, indicating that PEG200-PAA-Ca^{2+} had little effect on enhancing the friction between fibers. After being modified by M-STF, the friction between yarns was greatly improved. 27 wt% of M-STF could increase the F_{max} to 11.7 N (Fig. 7b). Different from that of neat Kevlar, the F_{max} of M-STF/Kevlar was rate-dependent: when the pull-out speed increased from 5 mm/min to 200 mm/min, the F_{max} increased from 10 N to 11.7 N. However, the increase in F_{max} was merely 1.7 N, which was much lower than 10 N, indicating that the increased friction between yarns was the main reason for the improvement of fabric strength. When the mass fraction of M-STF increased to 38 wt%, the yarns were completely wrapped by M-STF (Fig. 6d) and the F_{max} reached up to 26 N (Fig. 7d). Further increasing the mass fraction of M-STF, F_{max} did not increase too much (F_{max} for 52

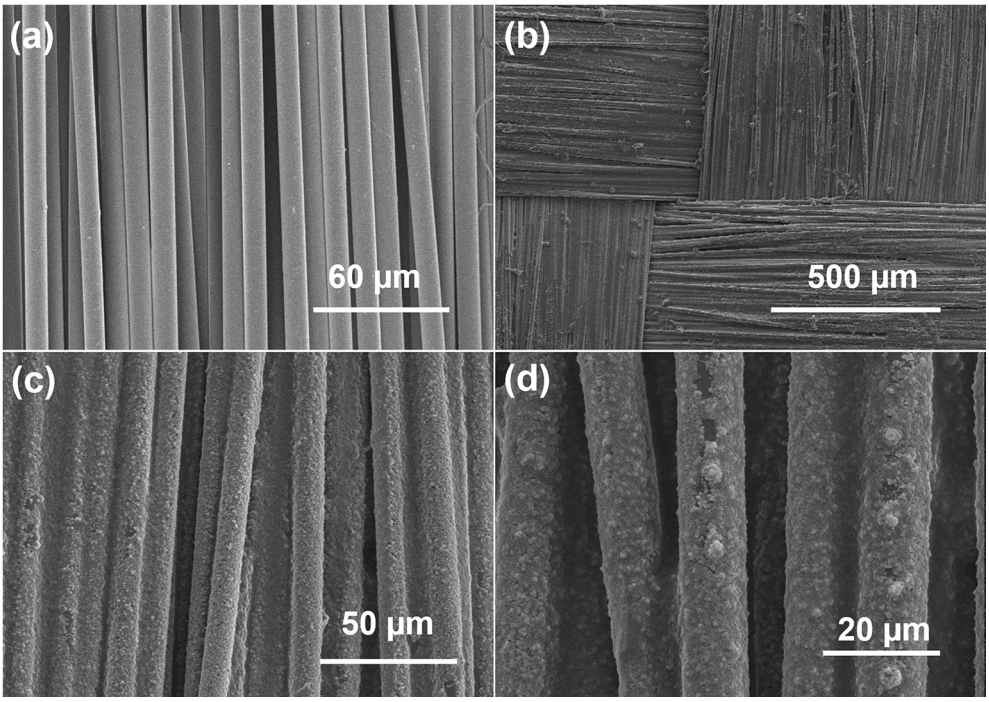

Fig. 6. SEM images of (a) neat Kevlar; (b), (c) and (d) M-STF/Kevlar.

wt% M-STF/Kevlar was 27.5 N, Fig. 7c), for the amount of STF on the fiber was saturated. However, too much M-STF would increase the weight of the fabric, which would restrict its practicality in flexible body protective area and reduce the industrial efficiency. Thus, the optimal mass fraction of M-STF in composite materials was 38 wt%. It should be pointed out that the mass fraction of STF in conventional STF reinforced Kevlar composite was usually up to 55 wt% ~ 75 wt% to achieve a good enhancing mechanical performance [10,33]. As a result, the composite could be heavy and its practical application would be limited. On the other hand, the F_{max} of conventional STF reinforced Kevlar composite was about 12 N [10,33–34], which was much lower than the 26 N in this work. Thus, M-STF/Kevlar showed promising applications in light-weight body protection for its low content of M-STF and super fabric reinforcement effect.

The yarn pull-out performance of 38 wt% M-STF/Kevlar treated at 55 °C was tested (Fig. 7e). Compared with the forces collected at room temperature (Fig. 7f), F_{max} did not change too much, demonstrating that it was friction instead of ST effect that improved the composite's mechanical properties. However, when Kevlar was treated by 50 vol% M-STF, a significant temperature-dependent effect could be observed. When the pull-out speed was 200 mm/min, the F_{max} was 4.5 N at 25 ℃, and it increased by 24.5% when the fabric was treated at 55 °C (Fig. 7g–i). Based on the above experimental results, the following conclusions could be drawn: 1) when Kevlar was impregnated by a high volume fraction of M-STF, increased friction between yarns was the main reason for the improvement of fabric strength, and ST effect could be ignored; As long as the concentration of M-STF was low, the influence of the ST effect could be obvious. 2) Overall, the fabric enhancement effect caused by the friction between particles was better than the counterpart that originated from the ST effect. The mechanism could be explained as follows: when the volume fraction of M-STF was high, the amount of dispersion medium was relatively small. Compared with particles, PEG200 would be preferentially adsorbed and spread on the surface of the yarn, leading to the separation of particles and liquid in M-STF and easier volatilization of PEG200. As a result, the ST effect almost disappeared while friction played a major role in reinforcing the fabric (Fig. 7j); however, when the concentration of STF was low and the amount of PEG200 was large enough to cover all particles and yarns, the ST effect would appear (Fig. 7j).

Thus, the safeguarding properties of M-STF/Kevlar under various mechanical conditions were systematically investigated. Firstly, force change of neat Kevlar and M-STF/Kevlar during penetration was collected by static puncture tests. As shown in Fig. 8a, the maximum contact force of neat Kevlar was 795 N, and it more than doubled (up to 1714 N) after being modified by M-STF, indicating that the impregnation of M-STF could enhance the puncture resistance of fabric. Drop hammer tests were employed to evaluate the anti-impact performance of M-STF/Kevlar (Fig. 8b–d). The maximum penetrating impact force of pure Kevlar was fluctuated around 1.5 kN and independent of the impact height. The maximum force of STF/Kevlar fabric was higher than that of neat Kevlar fabric, and because of the ST effect of M-STF, it increased slightly with the increasing impact height (When the drop height rose from 50 cm to 90 cm, the peak resistance increased from 1.8 kN to 1.9 kN). The mechanical properties enhancement of the composite was still ascribed to the increased friction between yarns. Besides, the increased friction between yarns could also improve the ballistic performance of the fabric. The residual velocities of the neat Kevlar and M-STF/Kevlar at different bullet-shooting impact speeds were shown in Fig. 8e. The relationship between the residual velocity and the incident velocity was fitted by the Recht-Ipson function [35]:

$$v_r = \alpha\left(v_i^p - v_{bl}^p\right)^{1/p}$$

where ν_i and ν_r were the incident velocity and residual velocity of the projectile, respectively; α and p were the parameters controlling the shape of the curve; ν_{bl} was the ballistic limit velocity. It was clear that the function fitted well with the experimental results. The ballistic limit velocity of M-STF/Kevlar was 122 m/s, which was significantly higher than the 90 m/s of neat Kevlar. Fig. 8f showed the dissipated energy of the neat Kevlar and M-STF/Kevlar. The dissipated energy E_{dis} was defined as:

$$E_{dis} = \frac{1}{2}mv_i^2 - \frac{1}{2}mv_r^2$$

where m was the mass of the bullet (2.08 g). Compared with neat Kevlar, the M-STF/Kevlar could dissipate more energy. As shown in Fig. 8g, when the incident velocity was 123 m/s, the neat Kevlar was

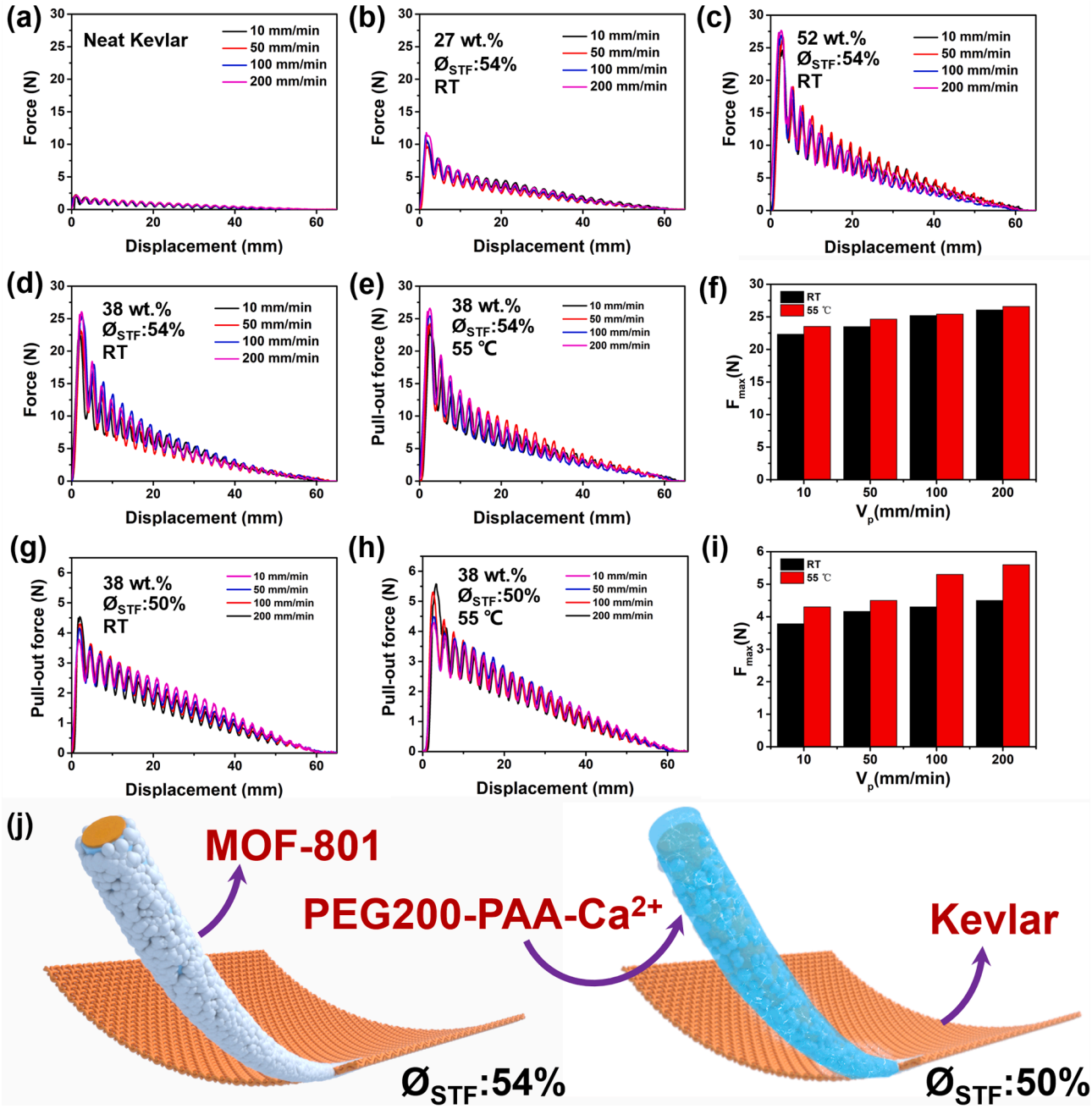

Fig. 7. Pull-out force vs. displacement at different pull-out speeds for (a) neat Kevlar, (b) 27 wt% M-STF (54 vol%)/Kevlar, (c) 52 wt% M-STF (54 vol%)/Kevlar, 38 wt% M-STF (54 vol%)/Kevlar (d) at room temperature and (e) treated at 55 ℃, 38 wt% M-STF (50 vol%)/Kevlar (g) at room temperature and (h) treated at 55 ℃. Pull-out speed and temperature dependent maximum pull-out force: (f) 38 wt% M-STF (54 vol%)/Kevlar and (i) 38 wt% M-STF (50 vol%)/Kevlar; (j) Schematic diagram of M-STF/Kevlar impregnated with different volume fraction of M-STF.

penetrated at 150 μs, while the penetrated time of M-STF/Kevlar extended to 200 μs, indicating that the addition of M-STF could significantly improve the ballistic performance of Kevlar.

4. Conclusions

In this work, inspired by the high-temperature resistance mechanism of thermophile proteins, a novel concentrated M-STF suspension was obtained by dispersing MOF-801 into PEG200-PAA-Ca^{2+}. Different from conventional STF which relied on the hydrogen bonds between dispersing phase and dispersing medium, the particles in M-STF are connected to dispersing medium through coordination. When the temperature rose, the synergistic effect of hydrophobic backbone of PAA and coordination between MOF-801 and PAA could enhance the interaction between particles and dispersing medium. As a result, the ST effect of M-STF became stronger which overcame the drawback of decreasing mechanical decrement of traditional STF at elevated-temperature. When the temperature rose to 55 ℃, particles in M-STF rearranged and connected to each other to form a M-frictional contact network, resulting in a liquid-to-solid transition of the suspension. Because of the liquid-to-solid transition, the initial storage modulus of the suspension increased from 13 Pa to 2036 Pa and a shapeable, self-healing, shear-stiffing, and conductive solid-like substance could be obtained. After being impregnated by M-STF, the mechanical properties of Kevlar could be greatly improved. In yarn pull-out tests, only 38 wt% M-STF could increase the maximum pull-out force from 2.2 N to 26 N,

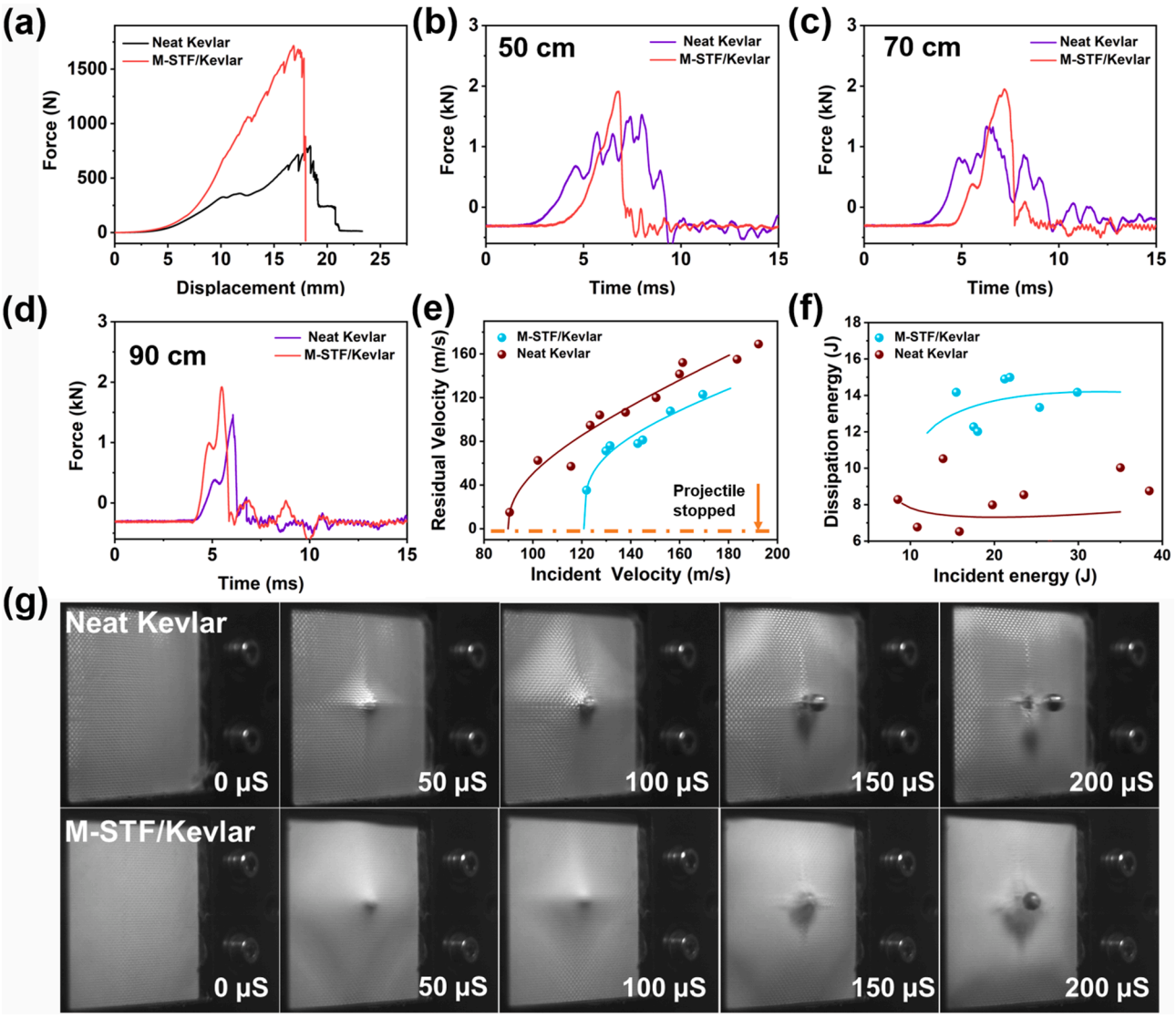

Fig. 8. (a) The puncture force curves of Neat Kevlar and M-STF/Kevlar. The resistance force of Neat Kevlar and M-STF/Kevlar under blunt impact with a falling height of (b) 50 cm, (c) 70 cm, and (d) 90 cm. (e) The residual velocity results of M-STF/Kevlar and neat Kevlar under high-speed shooting excitation and (f) the corresponding energy dissipation results. (g) The impact process of neat Kevlar and M-STF/Kevlar with an incident velocity of 123 m/s

indicating the composite had promising applications in lightweight body protection.

Declaration of Competing Interest

The authors declare that they have no known competing financial interests or personal relationships that could have appeared to influence the work reported in this paper.

Acknowledgment

Yuxuan Wu and Wenhui Wang contributed equally to this work. Financial supports from the National Natural Science Foundation of China (Grant No. 11972032, 11772320, 11802303, 11822209), USTC Research Funds of the Double First-Class Initiative (YD2480002004), the Strategic Priority Research Program of the Chinese Academy of Sciences (Grant No. XDB22040502), and the Open Project Program of Key Laboratory of Eco-textiles, Ministry of Education, Jiangnan University (No. KLET2012), are gratefully acknowledged.

Appendix A. Supplementary data

Supplementary data to this article can be found online at https://doi.org/10.1016/j.cej.2021.131793.

References

[1] K. Mochizuki, D. Ben-Amotz, Hydration-shell transformation of thermosensitive aqueous polymers, J. Phys. Chem. Lett. 8 (7) (2017) 1360–1364.
[2] Y. Tamai, H. Tanaka, K. Nakanishi, Molecular dynamics study of polymer–water interaction in hydrogels. 2. hydrogen-bond dynamics, Macromolecules 29 (21) (1996) 6761–6769.
[3] P. Linse, V. Lobaskin, Electrostatic attraction and phase separation in solutions of like-charged colloidal particles, Phys. Rev. Lett. 83 (20) (1999) 4208–4211.
[4] T. Nonoyama, Y.W. Lee, K. Ota, K. Fujioka, W. Hong, J.P. Gong, Instant thermal switching from soft hydrogel to rigid plastics inspired by thermophile proteins, Adv. Mater. 32 (2020), e1905878.
[5] X. Liu, J.L. Huo, T.T. Li, H.K. Peng, J.H. Lin, C.W. Lou, Investigation of the shear thickening fluid encapsulation in an orifice coagulation bath, Polymers (Basel) 11 (2019) 519.
[6] K. Liu, C.-F. Cheng, L. Zhou, F. Zou, W. Liang, M. Wang, Y.u. Zhu, A shear thickening fluid based impact resistant electrolyte for safe Li-ion batteries, J. Power Sources 423 (2019) 297–304.

[7] E. Brown, N.A. Forman, C.S. Orellana, H. Zhang, B.W. Maynor, D.E. Betts, J. M. DeSimone, H.M. Jaeger, Generality of shear thickening in dense suspensions, Nat. Mater. 9 (3) (2010) 220–224.
[8] A.F. Ávila, A.M. de Oliveira, S.G. Leão, M.G. Martins, Aramid fabric/nano-size dual phase shear thickening fluid composites response to ballistic impact, Compos. Part A Appl. Sci. Manuf. 112 (2018) 468–474.
[9] S. Gürgen, M.C. Kuşhan, W. Li, Shear thickening fluids in protective applications: A review, Prog. Polym. Sci. 75 (2017) 48–72.
[10] M. Liu, S. Zhang, S. Liu, S. Cao, S. Wang, L. Bai, M. Sang, S. Xuan, W. Jiang, X. Gong, CNT/STF/Kevlar-based wearable electronic textile with excellent anti-impact and sensing performance, Compos. Part A Appl. Sci. Manuf. 126 (2019), 105612.
[11] Q.-S. Wang, R.-J. Sun, M.u. Yao, M.-y. Chen, Y. Feng, The influence of temperature on inter-yarns fictional properties of shear thickening fluids treated Kevlar fabrics, Compos. Part A Appl. Sci. Manuf. 116 (2019) 46–53.
[12] J. Qin, B. Guo, L. Zhang, T. Wang, G. Zhang, X. Shi, Soft armor materials constructed with Kevlar fabric and a novel shear thickening fluid, Compos. B Eng. 183 (2020), 107686.
[13] E. Brown, H.M. Jaeger, Shear thickening in concentrated suspensions: phenomenology, mechanisms and relations to jamming, Rep. Prog. Phys. 77 (2014), 046602.
[14] R. Seto, R. Mari, J.F. Morris, M.M. Denn, Discontinuous shear thickening of frictional hard-sphere suspensions, Phys. Rev. Lett. 111 (2013), 218301.
[15] L.E. Edens, S. Pednekar, J.F. Morris, G.K. Schenter, A.E. Clark, J. Chun, Global topology of contact force networks: Insight into shear thickening suspensions, Phys. Rev. E 99 (2019), 012607.
[16] M. Hasanzadeh, V. Mottaghitalab, M. Rezaei, Rheological and viscoelastic behavior of concentrated colloidal suspensions of silica nanoparticles: A response surface methodology approach, Adv. Powder Technol. 26 (6) (2015) 1570–1577.
[17] C. Hu, J. Liu, Y. Wu, K.R. West, O.A. Scherman, Cucurbit [8] uril-regulated colloidal dispersions exhibiting photocontrolled rheological behavior, Small 14 (2018) 1703352.
[18] M. Liu, W. Jian, S. Wang, S. Xuan, L. Bai, M. Sang, X. Gong, Shear thickening fluid with tunable structural colors, Smart Mater. Struct. 27 (2018), 095012.
[19] K. Chen, Y. Wang, S. Xuan, S. Cao, X. Gong, Contribution of frictional contact during steady and oscillatory shear in the discontinuous shear thickening fluid, Smart Mater. Struct. 28 (2019), 045009.
[20] L.C. Hsiao, S. Jamali, E. Glynos, P.F. Green, R.G. Larson, M.J. Solomon, Rheological state diagrams for rough colloids in shear flow, Phys. Rev. Lett. 119 (2017), 158001.
[21] C.-P. Hsu, S.N. Ramakrishna, M. Zanini, N.D. Spencer, L. Isa, Roughness-dependent tribology effects on discontinuous shear thickening, P. Nat. Acad. Sci. 115 (20) (2018) 5117–5122.
[22] J.F. Morris, Lubricated-to-frictional shear thickening scenario in dense suspensions, Phys. Rev. Fluid 3 (2018), 110508.
[23] M. Wyart, M.E. Cates, Discontinuous shear thickening without inertia in dense non-brownian suspensions, Phys. Rev. Lett. 112 (2014), 098302.
[24] S. Pednekar, J. Chun, J.F. Morris, Simulation of shear thickening in attractive colloidal suspensions, Soft Matter 13 (9) (2017) 1773–1779.
[25] J. Warren, S. Offenberger, H. Toghiani, C.U. Pittman, T.E. Lacy, S. Kundu, Effect of temperature on the shear-thickening behavior of fumed silica suspensions, ACS Appl. Mater. Inter. 7 (33) (2015) 18650–18661.
[26] J. Qin, G. Zhang, Z. Ma, J. Li, L. Zhou, X. Shi, Effects of ionic structures on shear thickening fluids composed of ionic liquids and silica nanoparticles, RSC Adv. 6 (85) (2016) 81913–81923.
[27] X.-Q. Liu, R.-Y. Bao, X.-J. Wu, W. Yang, B.-H. Xie, M.-B. Yang, Temperature induced gelation transition of a fumed silica/PEG shear thickening fluid, RSC Adv. 5 (24) (2015) 18367–18374.
[28] X. Zhang, T. Zhang, Y. Wang, J. Li, C. Liu, N. Li, J. Liao, Mixed-matrix membranes based on Zn/Ni-ZIF-8-PEBA for high performance CO2 separation, J. Membrane Sci. 560 (2018) 38–46.
[29] M. He, L. Wang, Y. Lv, X. Wang, J. Zhu, Y. Zhang, T. Liu, Novel polydopamine/metal organic framework thin film nanocomposite forward osmosis membrane for salt rejection and heavy metal removal, Chem. Eng. J. 389 (2020), 124452.
[30] R.C. Dougherty, Temperature and pressure dependence of hydrogen bond strength: A perturbation molecular orbital approach, J. Chem. Phys. 109 (1998) 7372–7378.
[31] T.I. Mizan, P.E. Savage, R.M. Ziff, Temperature dependence of hydrogen bonding in supercritical water, J. Phys. Chem. 100 (1) (1996) 403–408.
[32] E. Tapie, Y.B. Guo, V.P.W. Shim, Yarn mobility in woven fabrics – a computational and experimental study, Int. J. Solids Struct. 80 (2016) 212–226.
[33] J. Zhang, Y. Wang, J. Zhou, C. Zhao, Y. Wu, S. Liu, X. Gong, Intralayer interfacial sliding effect on the anti-impact performance of STF/Kevlar composite fabric, Compos. Part A-Appl. S 145 (2021), 106401.
[34] S. Cao, H. Pang, C. Zhao, S. Xuan, X. Gong, The CNT/PSt-EA/Kevlar composite with excellent ballistic performance, Compos. Part B-Eng. 185 (2020), 107793.
[35] R.F. Recht, T.W. Ipson, Ballistic perforation dynamics, J. Appl. Mech. 30 (1963) 384–390.